

Parabolic Resonance: A Route to Hamiltonian Spatiotemporal Chaos

Eli Shlizerman* and Vered Rom-Kedar†

Faculty of Mathematics and Computer Science, Weizmann Institute of Science, Post Office Box 26, Rehovot 76100, Israel
(Received 18 May 2008; published 20 January 2009)

We show that initial data near an unperturbed *stable* plane wave can evolve into a regime of spatiotemporal chaos in the slightly forced conservative periodic one-dimensional nonlinear Schrödinger equation. Statistical measures are employed to demonstrate that this spatiotemporal chaos is intermittent: there are windows in time for which the solution gains spatial coherence. The parameters and initial profiles that lead to such intermittency are predicted by utilizing a novel geometrical description of the integrable unforced equation.

DOI: 10.1103/PhysRevLett.102.033901

PACS numbers: 42.65.Sf, 05.45.-a, 45.20.Jj, 52.35.Mw

The appearance of chaos in deterministic spatially dependent systems dates back to Lorenz, who showed that a set of three ordinary differential equations, describing the simplified dynamics of rolls in the Rayleigh-Bénard convection system, can exhibit irregular behavior. This understanding led to theoretical and experimental studies of various spatially-dependent systems that exhibit temporal chaos. Then, an even more intriguing behavior called *spatiotemporal chaos* (STC) was identified: chaotic dynamics that involve variations in *both* time and space. Such behavior is commonly characterized by finding both positive Lyapunov exponents (temporal chaos) and a rapid decay of the time average of the two-points spatial correlation function (spatial decoherence) [1,2]. The phenomenon of STC was experimentally observed in a variety of systems such as convection experiments [3], rotating convection [4], chemical reaction-diffusion [5] and colonies of microorganisms [6]. Theoretically, STC was shown to exist in dissipative models such as the Kuramoto-Sivashinsky [7], complex Ginzburg-Landau [8] and the forced and damped nonlinear Schrödinger (NLS) [2,9] equations. In the one-dimensional setting, these dissipative systems have finite dimensional attractors, and their dimension typically increases with the systems spatial length L . Such systems with large dimensional attractors were shown to exhibit STC [8,10]. Notably, STC can also arise in systems with finite length L and low-dimensional attractors: the dynamics is governed then by only a few modes having chaotic amplitudes and relative phases [2].

In this context, the forced and damped NLS equation was proposed to be a prototypical model. On one hand, its attractor dimension increases with L , and on the other, STC is observed for short spatial lengths: when the attractor has more than three modes STC already emerges [2]. Using modulation instability theory, a critical length scale L_c , which is independent of the damping and forcing rates, is identified (details follow): For $L > L_c$ the attractor dimension exceeds three, thus, in the forced and damped case STC should appear. Conversely, for $L < L_c$, only temporal chaos was observed [2].

Here we address the appearance of STC in small Hamiltonian systems ($L < L_c$) by studying the conservative ac-driven periodic NLS equation. Since there is no attractor here, there is no obvious low-dimensional mechanism that governs the motion. Indeed, for the same parameter values different solutions may exhibit regular behavior, temporal-chaos and even STC (large amplitude unperturbed solutions typically have many unstable modes and thus, with forcing, exhibit STC). Yet, one may expect that for small forcing and small amplitude nearly flat initial data, the evolution will remain spatially coherent at least for $L < L_c$ (as in [2]). In this Letter, we show that this is not the case: STC may appear even when $L < L_c$. In fact, by changing only one parameter, the forcing frequency, the evolution of such an initial profile can be altered from being regular to being STC.

The focusing periodic 1D NLS perturbed by an ac-driver $\varepsilon e^{i\Omega^2 t}$ with a frequency Ω^2 (see [11,12] and references therein) may be transformed to the autonomous NLS equation with a constant potential [13,14]:

$$i\Psi_t - \Psi_{xx} - (g|\Psi|^2 - \Omega^2)\Psi = \varepsilon, \quad \Psi(x, 0) = \Psi_0(x), \quad (1)$$

where hereafter $\Psi(x, t) = \Psi(x + L, t)$, $x \in \mathbb{R}$, $g = 2$ and $\Psi_0(x)$ denotes the initial data profile. We consider here the Hamiltonian case, so the linear damping term of [2,11,13,15], $-i\delta\Psi$, is omitted. The unperturbed equation ($\varepsilon = 0$) is integrable. Its simplest kind of solutions are the plane waves: $\Psi_{\text{PW}}(t; M_{\text{PW}}, E_0) = \sqrt{M_{\text{PW}}} \exp[iE_{\text{PW}}t - iE_0]$, with mass M_{PW} and frequency $E_{\text{PW}} = \Omega^2 - gM_{\text{PW}}$. The plane wave is called resonant when $E_{\text{PW}} = 0$, namely, when its mass is $M_{\text{PW-res}} = \Omega^2/g$. Modulation stability analysis shows that for $M_{\text{PW}} \in \frac{1}{2g}(\frac{2\pi}{L})^2(j^2, (j+1)^2) = (M_{j\text{LUM}}, M_{(j+1)\text{LUM}})$ and $j \geq 1$, the plane waves have j linearly unstable modes (LUM) [16]. We call the stable plane waves with 0 LUM *elliptic* ($M_{\text{PW}} < M_{1\text{LUM}}$), the unstable ones with 1 LUM *1-hyperbolic* ($M_{1\text{LUM}} < M_{\text{PW}} < M_{2\text{LUM}}$), and the bifurcating from 0 to 1 LUM *1-parabolic* ($M_{\text{PW}} = M_{1\text{LUM}}$). The *1-hyperbolic* plane waves have families of homoclinic orbits—solutions with non-

trivial spatial structure that asymptote to the plane waves as $t \rightarrow \pm\infty$ [11].

When both damping and forcing are considered as in [2,11,13,15], spatially flat solutions tend to synchronize with the forcing frequency and converge to a resonant plane wave with amplitude $\sqrt{M_{\text{PW-res}}}$. Then, it is observed that the number of modes that govern the dynamics is essentially given by the number of LUMs of the unperturbed synchronous plane wave plus one (the flat mode) [2]. Thus, when this plane wave has only one LUM, a two mode Galerkin truncation of the system (taking $\Psi(x, t) = c(t) + b(t) \cos \frac{2\pi x}{L}$, where c, b are the complex amplitudes of the first two modes) provides a good approximation of the full dynamics [13,15]. Then, only temporal-chaotic solutions associated with the plane wave homoclinic orbits may appear (see [17–19] for the truncated model analysis). Once the synchronous plane wave has *two* or more LUMs, namely $M_{\text{PW-res}} \geq M_{2\text{LUM}}$ and thus $L \geq L_c = 2\sqrt{2}\pi/\Omega$, STC is observed [2,9].

In contrast, in the conservative periodic case, the solutions do not converge to a low-dimensional attractor. Instead, for any given set of parameters, a variety of regular and chaotic solutions coexist. Previously, we demonstrated that for small forcing, solutions evolving from *symmetric* initial data close to plane wave with $M_{\text{PW}} < M_{2\text{LUM}}$, can be classified into three types of *temporal* chaos. Moreover, these solutions are similar in structure to the solutions of the two mode Galerkin truncation of the conservative model [14,19]. In particular, it was observed that when

the one-parabolic plane wave is resonant, namely $M_{\text{PW-res}} = M_{1\text{LUM}}$, hence, $\Omega^2 = \Omega_{\text{pr}}^2 = \frac{1}{2}(\frac{2\pi}{L})^2$, symmetric profiles that are initialized near this plane wave exhibit a new type of temporal-chaotic dynamics that was called parabolic resonance chaos [14]. Here we consider nearly flat and *asymmetric* initial profiles and show that the parabolic resonance mechanism can lead to spatial decoherence. We provide a novel geometrical interpretation and characterization for this development of STC. Furthermore, we show that STC can appear even when the profile is initialized near an *unperturbed stable plane wave* (0 LUMs) and the forcing is small.

Figures 1(a)–1(c) presents the evolution of such an initial profile ($M(\Psi(x, 0)) < M_{1\text{LUM}} = 0.2025$) under Eq. (1) for three different forcing frequencies, where all other parameters are identical. In particular, $L = \frac{2\pi}{0.9} < L_c(\Omega)$ for all the three frequencies, namely, the resonant plane wave has always less than two LUM [$M_{\text{PW-res}}(\Omega) < M_{2\text{LUM}} = 0.81$]. In the first row the evolution of the three surfaces $|\Psi(x, t)|$ is shown. Notice that only in the middle plot, at which the frequency was tuned to be in parabolic resonance, spatial decoherence seems to emerge. Figure 2 demonstrates that the parabolic resonant solution is indeed the most decoherent, having the smallest time averaged spatial autocorrelation. Moreover, it shows that the decoherence is *intermittent*—it has windows at which spatial correlation is regained on observable time scales (these appear also in dissipative STC systems [7,8]). This intricate behavior is better understood by examining

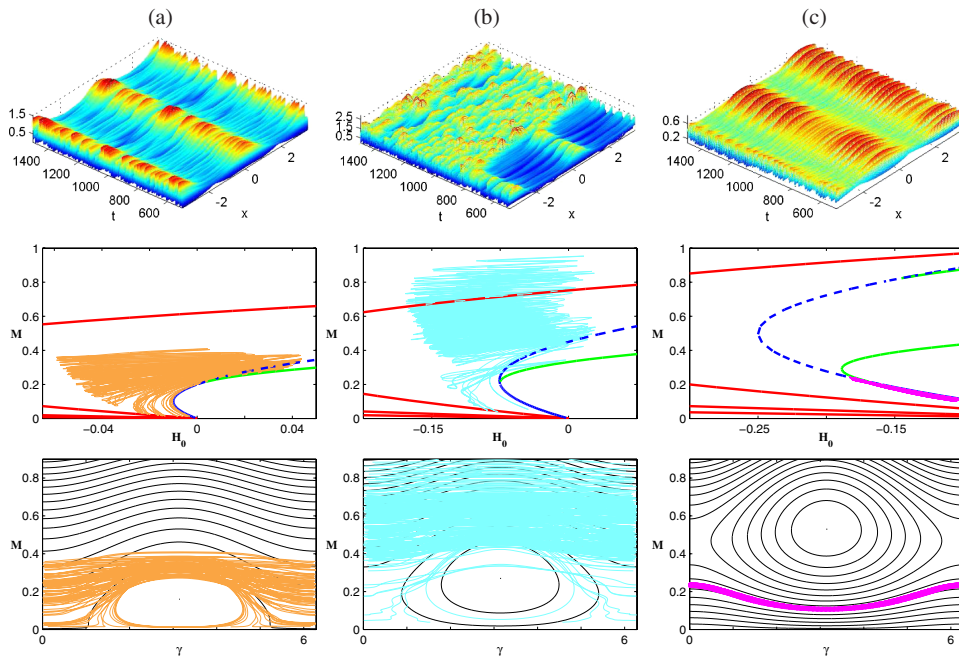


FIG. 1 (color online). Evolution of a nearly flat profile under forcing with three different frequencies: (a) elliptic: $\Omega^2 = 0.2$ (b) parabolic: $\Omega^2 = 0.45$ and (c) hyperbolic: $\Omega^2 = 1$. First row: surface plot, $|\Psi(x, t)|$, Second row: PDE-EMBD: blue, green, and red curves: projections of unperturbed standing waves branches to the (M, H_0) space. Orange, cyan, and magenta lines: projections of the perturbed solutions: $(M(\Psi(x, t)), H_0(\Psi(x, t)))$. Third row: projections to the $(M(\Psi(x, t)), \gamma = \arg((\Psi(x, t))_x))$ space on top of the H_{flat} level lines (black). The initial profile is $\Psi_0(x) = \sqrt{0.15}e^{i5/9\pi} + 10^{-3}e^{i(2\pi/L)x}$, $\varepsilon = 5 \times 10^{-2}$, $\frac{2\pi}{L} = 0.9$.

two additional projections. Recall that the first two integrals of the unperturbed equation are its mass (particle number), and the unperturbed Hamiltonian:

$$\begin{aligned} M(\Psi) &= \frac{1}{L} \int_{-L/2}^{L/2} |\Psi|^2 dx, \\ H_0(\Psi) &= \frac{1}{L} \int_{-L/2}^{L/2} \left(-|\partial_x \Psi|^2 + \frac{g}{2} |\Psi|^4 - \Omega^2 |\Psi|^2 \right) dx, \end{aligned} \quad (2)$$

so, in particular, $M(\Psi_{PW}(t)) = M_{PW}$. For the perturbed solutions both $M(\Psi(x, t))$ and $H_0(\Psi(x, t))$ become time-dependent (second row of Fig. 1). While $|H_0(\Psi(x, t)) - H_0(\Psi(x, 0))| = O(\varepsilon)$ for all time [20], the mass $M(t)$ of the parabolic resonant solution (middle column) is ramped up by the ac driver. We propose that this ramping up of M provides a low-dimensional mechanism for the development of STC; The parabolic resonance instability ramps M up beyond the threshold value of M_{2LUM} , there, three modes are activated, and thus STC appears. The intermittent behavior (see Fig. 2) appears when the mass occasionally decreases back to the values of $M < M_{2LUM}$ where spatial coherence is gained.

The underlying skeleton shown in the second row of Fig. 1 is the PDE-EMBD—the Energy Momentum Bifurcation diagram. We propose that projecting the perturbed solutions on top of this skeleton provides novel insights regarding their structure. The skeleton consists of the projection of the simplest unperturbed solutions of Eq. (1) to the (H_0, M) plane. The blue curves in Figs. 1 and 3 correspond to the plane wave family: $\{M_{PW} = \frac{(\Omega^2 - E_{PW})}{g}, H_0 = \frac{g}{2} M_{PW}^2 - \Omega^2 M_{PW}\}$. For $M_{PW} > M_{1LUM}$ its homoclinic orbits have the same projection indicated by a dashed blue

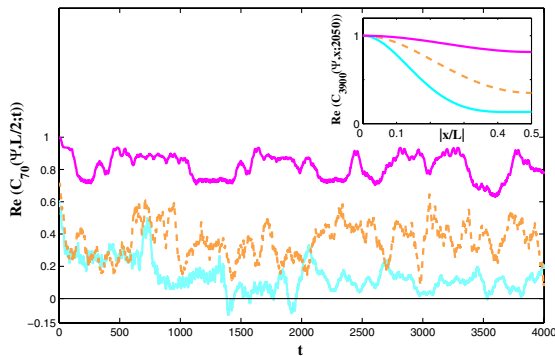


FIG. 2 (color online). The normalized averaged autocorrelation function, $C_T(\Psi, y; t) = \int_{t-T/2}^{t+T/2} \int_{-L/2}^{L/2} \Psi(x, s) \Psi^*(x + y, s) dx ds / \int_{t-T/2}^{t+T/2} \int_{-L/2}^{L/2} |\Psi(x, s)|^2 dx ds$ is calculated over a time window T for the three solutions of Fig. 1 with the elliptic (orange), parabolic (cyan) and hyperbolic (magenta) frequencies. Inset: Long-time average of the normalized correlations $\text{Re}[C_{3900}(\Psi, x; 2050)]$ (here $\text{Im}[C_{3900}(\Psi, x; 2050)] \approx 0$). It shows that for large T , the parabolic resonant solution is the most decoherent of the three. Similar results are found using the mutual information measure (see [2,11]). Main figure: temporal changes of the normalized correlations at the midbox point: $\text{Re}[C_{70}(\Psi, L/2; t)]$.

curve. The red and green curves correspond to the standing waves solutions: $\Psi_{sw}(x, t) = e^{iEt + iE_0} \Phi_E(x)$, where E , $\Phi_E(x)$ are eigenvalues and eigenfunctions of the nonlinear operator $\mathcal{N}(\Phi_E)\Phi_E = (\partial_{xx} + g|\Phi_E|^2 - \Omega^2)\Phi_E = -E\Phi_E$ satisfying $\Phi_E(x + L) = \Phi_E(x)$. Notably, these solutions are found analytically: the equation $\mathcal{N}(\Phi_E) - E\Phi_E = 0$, viewed as an initial value problem in x , is the Duffing equation. Imposing the L periodicity in x leads to the selection of a discrete set of solution branches.

The PDE-EMBD provides a convenient representation of these branches of solutions. Since the unperturbed equation is integrable and M and H_0 are preserved, any unperturbed solution projected to the PDE-EMBD produces a single point (Fig. 3). If this point is bounded away from a particular branch then their corresponding profiles are distinct. The key observation here is that for the periodic 1D NLS, the diagram consists of curves that are typically well separated (only a few projection-produced overlaps and intersections appear). Hence, it enables to distinguish between neighborhoods of the different standing waves (and similarly of the traveling waves) solutions; Projecting a perturbed solution on top of this integrable skeleton helps to identify the regions in the infinite dimensional phase space that it visits; In the hyperbolic frequency case [Fig. 1(c)], the solution mainly remains near the stable plane wave regime (solid blue curve) and thus appears regular. In the elliptic frequency case [Fig. 1(a)] the solution crosses the unstable plane wave branch (dashed blue curve), hence exhibits temporal chaos that is associated with the plane wave homoclinic orbits. In the parabolic case [Fig. 1(b)], the solution wanders away from the plane wave curve along the green standing wave branch and the homoclinic crossings till its mass is ramped up to levels at which STC appears.

Finally, we show that the classification of solutions that are initialized near the plane waves depends on both the number of LUMs associated with them (determined by their mass) and on their phases. First, recall that spatially flat solutions of the form $\Psi(x, t) = \sqrt{M(t)} \exp[i\gamma(t)]$ are invariant under the perturbed dynamics and that the motion

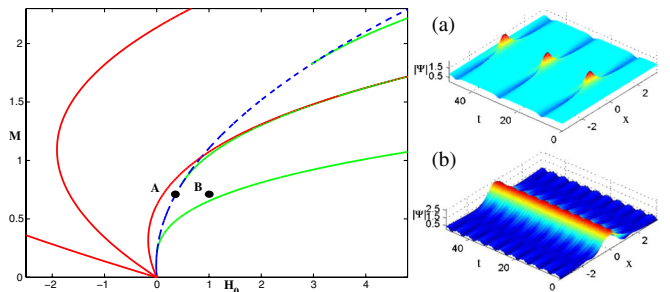


FIG. 3 (color online). (left) The PDE-EMBD: blue, green, and red curves projections of three standing waves families to the (H_0, M) space. Black points: projections of the two quasiperiodic solutions shown on the right. (a) (top): solution that is close to the plane wave homoclinic orbits. (b) (bottom) solution that is close to a stable standing wave branch.

on this “flat” invariant plane is described by the Hamiltonian $H_{\text{flat}}(M, \gamma) = \frac{g}{2}M^2 - \Omega^2 M + 2\varepsilon\sqrt{M}\cos\gamma$ [11,12]. H_{flat} has a resonance zone near the unperturbed resonant plane wave $M_{\text{PW-res}}$ of width of order $\sqrt{\varepsilon}$ in M . The third row of Fig. 1, showing the level sets of H_{flat} , demonstrates that the chosen ε value is sufficiently small such that the resonance zone lies entirely below $M_{2\text{LUM}}$ for both the elliptic and parabolic frequencies. The motion in the neighborhood of this “flat” invariant plane depends on the value of M : for small values it is stable, for $M \in (M_{\text{ILUM}}, M_{2\text{LUM}})$ it is unstable and exhibits excursions along the unperturbed homoclinic orbits to the plane wave, whereas for $M > M_{2\text{LUM}}$ we expect STC to appear. Indeed, compare the H_{flat} level sets with the projection of the solutions to the $(M, \gamma = \arg\langle\Psi(x, t)\rangle_x)$ plane; In the elliptic and hyperbolic [21] cases the level sets of H_{flat} are essentially traced by the solutions (first and third columns): only when $M \in (M_{\text{ILUM}}, M_{2\text{LUM}})$ the chaotic homoclinic excursions appear as straight horizontal lines in the (M, γ) plane. On the other hand, in the parabolic case, we see that the perturbed motion of a nearly flat profile leads to ramping up of M much beyond the $\sqrt{\varepsilon}$ resonance zone of the perturbed flat solutions. The parabolic resonant instability drives the solutions away from the flat invariant plane. This instability is sufficiently large to drive the particle number beyond the critical value of $M_{2\text{LUM}}$, and thus spatial decoherence is observed.

This last row reveals an intricate relation between the choice of the forcing frequency Ω^2 , the forcing amplitude ε and the nearly flat initial data (mass and phase); we demonstrated that we can predict how to alter these to produce different perturbed solutions. In particular, to drive a small nearly flat initial profile to STC, it is best to tune Ω^2 to be close to Ω_{pr}^2 and then increase ε till decoherence is achieved. We conjecture that for any given set of parameters $(\frac{2\pi}{L}, g)$ there exist $\varepsilon_{\text{min}} = \varepsilon_{\text{min}}(\frac{2\pi}{L}, g)$ such that for all $\varepsilon > \varepsilon_{\text{min}}$ there exists an order one interval of initial phases and an $\mathcal{O}(\sqrt{\varepsilon})$ interval of $(\Omega^2 - \Omega_{\text{pr}}^2)$ values that drive an arbitrarily small amplitude solution to a spatial decoherent state. We demonstrated that ε_{min} is rather small [$\varepsilon_{\text{min}}(0.9, 2) \approx 0.05$]. Conversely, coherence for long time scales may be gained by either decreasing ε or by selecting Ω^2 away from this $\mathcal{O}(\sqrt{\varepsilon})$ interval.

The implications of our findings on experiments (e.g., of the dependence of the appearance of STC on the driver frequency) is yet to be explored; recent experiments with high intensity laser beams [22] or Bose-Einstein condensates [23] confined in a cigar-shaped [24] or in magnetically guided ring-shaped traps [25], are often modeled by the integrable 1D NLS. Designing these experiments with an ac driver with an externally tunable variable frequency to examine the emergence of STC may be exciting and may lead to better control of such devices. Moreover, it may shed light on the dynamical stability of current experiments as the 1D NLS equation models only their leading order effects [22,26].

We acknowledge the support of the Israel Science Foundation (273/07), Minerva foundation, and Russian-Israeli grant (06-01-72023). We thank J. Gibbon, A. Soffer, E. Titi, D. Turaev, and M. Weinstein for helpful discussions.

*eli.shlizerman@weizmann.ac.il

†vered.rom-kedar@weizmann.ac.il

- [1] M. C. Cross and P. C. Hohenberg, Rev. Mod. Phys. **65**, 851 (1993), and references therein.
- [2] D. Cai *et al.*, Phys. Lett. A **253**, 280 (1999).
- [3] G. Ahlers and R. P. Behringer, Phys. Rev. Lett. **40**, 712 (1978); P. Bergé, Phys. Scr. **40**, 381 (1989).
- [4] L. Ning *et al.*, Phys. Rev. Lett. **71**, 2216 (1993); M. C. Cross and P. C. Hohenberg, Science **263**, 1569 (1994).
- [5] Q. Ouyang and J.-M. Flesselles, Nature (London) **379**, 143 (1996).
- [6] K. J. Lee, Phys. Rev. Lett. **76**, 1174 (1996).
- [7] P. Manneville, *Dissipative Structures and Weak Turbulence* (Academic Press, San Diego, 1990), and references therein.
- [8] M. P. Fishman and D. A. Egolf, Phys. Rev. Lett. **96**, 054103 (2006).
- [9] M. J. Ablowitz *et al.*, Math. Comput. Simul. **43**, 3 (1997).
- [10] D. A. Egolf *et al.*, Nature (London) **404**, 733 (2000).
- [11] D. Cai *et al.*, *Handbook of Dynamical Systems* (Elsevier, New York, 2002), Vol. 2, p. 599.
- [12] G. Haller, *Chaos Near Resonance*, Applied Mathematical Sciences Vol. 138 (Springer-Verlag, NY, 1999).
- [13] A. R. Bishop *et al.*, Phys. Lett. A **144**, 17 (1990).
- [14] E. Shlizerman and V. Rom-Kedar, Phys. Rev. Lett. **96**, 024104 (2006).
- [15] N. Ercolani *et al.*, Physica (Amsterdam) **43D**, 349 (1990).
- [16] In the unperturbed case, due to integrability, the evolution of nearly flat initial data is regular even when it is initialized near a linearly unstable plane wave. Then, it follows closely the plane wave homoclinic orbits, see Fig. 3. Yet, numerical errors can ruin integrability [9].
- [17] G. Haller and S. Wiggins, Physica (Amsterdam) **85D**, 311 (1995).
- [18] G. Kovacic and S. Wiggins, Physica (Amsterdam) **57D**, 185 (1992).
- [19] E. Shlizerman and V. Rom-Kedar, Chaos **15**, 013107 (2005).
- [20] Define $H_1(\Psi) = \frac{1}{L} \int (\Psi^* e^{i\theta} + \Psi e^{-i\theta}) dx$ and note that the total Hamiltonian $H_T(\Psi) = H_0(\Psi) + \varepsilon H_1(\Psi)$ is conserved and that $H_1(\Psi)$ is bounded.
- [21] Here, in the hyperbolic frequency case, the initial amplitude lands below the resonance zone and thus the motion is mostly regular.
- [22] J. Moloney and A. Newell, *Nonlinear Optics* (Advanced Book Program, Boulder, CO, 2004).
- [23] M. H. Anderson *et al.*, Science **269**, 198 (1995); K. B. Davis *et al.*, Phys. Rev. Lett. **75**, 3969 (1995).
- [24] V. Dunjko *et al.*, Phys. Rev. Lett. **86**, 5413 (2001).
- [25] S. Gupta *et al.*, Phys. Rev. Lett. **95**, 143201 (2005); J. A. Sauer *et al.*, Phys. Rev. Lett. **87**, 270401 (2001); M. Key *et al.*, Phys. Rev. Lett. **84** 1371 (2000).
- [26] L. Friedland and A. Shagalov, Phys. Rev. Lett. **81**, 4357 (1998).